Wiley
International Journal of Antennas and Propagation
Volume 2024, Article ID 7893488, 15 pages
https://doi.org/10.1155/ijap/7893488

WILEY

Research Article

Decoupling Structure for High-Bandwidth Multiport Monopole Antennas in K-Band and 5G Applications

Daniyal Ali Sehrai,[1] **Saad Hassan Kiani**,[2] **Tanweer Ali**,[3] **Muhammad Inam Abbasi**,[2] **Muhammad Ramlee Kamarudin**,[4] **Abeer D. Algarni**,[5] **and Hela Elmannai**[5]

[1]*Department of Electric, Electronic and Communication Engineering, Public University of Navarre (UPNA), Arrosadia Campus, Pamplona 31006, Spain*
[2]*Centre for Telecommunication Research & Innovation (CETRI), Faculty of Electronic and Computer Engineering and Technology (FTKEK), Universiti Teknikal Malaysia Melaka (UTeM), Melaka 76100, Malaysia*
[3]*Department of Electronics and Communication Engineering, Manipal Institute of Technology, Manipal Academy of Higher Education, Manipal 576104, India*
[4]*Faculty of Electrical and Electronic Engineering, Universiti Tun Hussein Onn Malaysia, Batu Pahat 86400, Johor, Malaysia*
[5]*Department of Information Technology, College of Computer and Information Science, Princess Nourah bint Abdulrahman University, P.O. Box 84428, Riyadh 11671, Saudi Arabia*

Correspondence should be addressed to Muhammad Inam Abbasi; inamabbasi@utem.edu.my

Received 4 September 2024; Accepted 11 December 2024

Academic Editor: Giovanni Magno

This paper introduces a multiport monopole antenna featuring high isolation and a broad operating bandwidth, specifically designed for K-band and 5 G applications. The proposed antenna configuration comprises four antenna elements assembled to achieve a compact design. A 0.254 mm thick Rogers RT-5880 substrate is used, with an overall size of 24 × 22 mm. Each antenna element is supported by a truncated ground plane, and four symmetrical slots are introduced into the radiating structures. As a result, the proposed multiport antenna covers a frequency band of approximately 18–27 GHz, based on the −10 dB criterion, providing a wide bandwidth of nearly 9 GHz. The separation between the antenna elements is about 4.5 mm. Additionally, a decoupling structure is inserted between the radiating elements to enhance isolation within the desired band, also resulting in a minor improvement in the operating bandwidth. Several performance metrics, including total active reflection coefficient (TARC), diversity gain (DG), envelope correlation coefficient (ECC), and channel capacity loss (CCL), are evaluated and show satisfactory performance within the operating bandwidth. The proposed antenna achieves more than 75% radiation efficiency. The overall performance of the multiport antenna indicates its potential for K-band and 5 G applications.

Keywords: 5G; decoupling; ECC; K-band; monopole; multiport antenna; wideband

1. Introduction

Due to the growing traffic on communication networks and the demand for higher data rates and bandwidth, 5 G has garnered significant attention. The 5 G communication spectrum is divided into two portions: mm-wave and Sub-6 GHz bands. In the Sub-6 GHz frequency band, spectrum congestion presents a challenge below 6 GHz [1]. This is because many services pre-existing before 5 G, such as Bluetooth, Wi-Fi, WiMAX, and various IEEE standards, have already utilized substantial portions of this spectrum [2]. Additionally, the predecessors of 5 G are located near the

5 G Sub-6 GHz spectrum [3]. As a result, achieving wideband coverage requires dedicating many channels as guard bands to minimize interference.

In contrast, the mm-wave or high-frequency portion of the spectrum offers a larger bandwidth compared to Sub-6 GHz, as most of the mm-wave bands are less utilized and have fewer transmission interference problems [4, 5]. For 5 G applications, the 24.5–27.5 GHz frequency band is allocated [6], while the K-band, ranging from 18 to 27 GHz, is preferred for some short-range applications [7, 8]. Moreover, using multiple antennas can enhance performance by mitigating attenuation issues at these high frequencies [9]. However, when multiple antennas share a common substrate, mutual coupling can become a severe problem [10]. High mutual coupling between antenna elements can degrade signal integrity, so careful assembly is necessary to maintain low mutual coupling.

In antenna arrays, elements are excited by a common source, whereas in antenna systems, each element is excited by separate sources. While antenna arrays can achieve high gain through multiple antennas [11], they also increase the antenna size and present challenges in minimizing mutual coupling. Additionally, power dividers used in antenna arrays can introduce losses. Metamaterials have been shown to improve radiation performance and isolation [12], but they require large surface areas due to their periodic structures [13]. Similarly, incorporating various decoupling structures with antennas can enhance isolation [14].

For example [15], presents a decoupling structure with four strips of equal length connected by a hollow circular stripe to improve isolation at two mm-wave frequency bands. This configuration is supported by a full ground plane, but our focus is on improving isolation across a wide operating bandwidth using a truncated ground plane. Our decoupling structure includes four strips of varying lengths—two shorter and two longer—connected by a common circular structure. The impact of these different-length strips is discussed. A compact UWB antenna with four ports, described in [16], features a mesh-like decoupling structure with a defected ground structure (DGS) to improve isolation and realize a wide bandwidth from 4.5 to 16.4 GHz, with isolation exceeding 20 dB. The overall volume is $45 \times 45 \times 1.6\,\text{mm}^3$. In [17], a multiport antenna for the Ka-band, covering 24.1–30.9 GHz, is proposed, achieving more than 30 dB isolation and an utmost gain of 6.5 dBi, with a compact overall size of $35 \times 40\,\text{mm}^2$. Another two-port antenna in [18] has an overall size of $11.4 \times 5.3\,\text{mm}^2$, providing a gain of 6 dBi with a bandwidth of 0.8–1.0 GHz centered at 29 GHz, and an isolation greater than 36 dB. This isolation is improved by introducing slots in the radiators and tilting them by 45°. In [19], a two-port antenna with dimensions of $20.5 \times 12\,\text{mm}^2$ operates within a bandwidth of 25.5–30 GHz, providing a peak gain of 8.75 dBi and achieving isolation ranging from 32 to 43 dB. In [20], a four-port antenna covers 25.5–29.6 GHz, with an isolation of 17 dB, an envelope correlation coefficient (ECC) of less than 0.01, and a peak gain of 8.3 dBi, all within a PCB size of $30 \times 35\,\text{mm}^2$. Another four-port antenna described in [21] operates from 27 to 29.4 GHz, offering isolation greater than 29 dB, an ECC of less than 0.16, and a gain of 6.1 dBi, with dimensions of $30 \times 30\,\text{mm}^2$. In [22], a two-port antenna with a size of $52 \times 23\,\text{mm}^2$ functions across 24–30 GHz, achieving isolation above 24 dB, an ECC below 0.0013, and a peak gain of 12.4 dBi. The two-port antenna presented in [23] has an overall size of $26 \times 11\,\text{mm}^2$, covering 26–29 GHz and 36–41 GHz, with isolation varying from 25 to 70 dB and 20–35 dB in the respective bands, and gains of 5 and 5.7 dBi. Lastly [24], describes a two-port antenna with dimensions of $53 \times 31.7\,\text{mm}^2$, operating in the 22.5–50 GHz range, achieving more than 20 dB of isolation, an ECC of 0.12, and a peak gain of 15 dBi, facilitated by an electromagnetic bandgap (EBG) reflector.

Overall, the proposed designs in the literature face challenges with bandwidth and compactness, often struggling with low isolation levels. In this article, we present a wideband multiport antenna with a compact size for K-band and 5 G applications. The proposed antenna features improved bandwidth and enhanced decoupling between antenna elements to ensure strong performance for both transmission and reception.

Some key contributions of the proposed work are:

1. Our proposed antenna covers the entire K-band (18–27 GHz), suitable for short-range applications, and also includes the 5 G band (24.5–27.5 GHz) within its operating bandwidth.
2. The antenna's bandwidth is enhanced through the strategic positioning and assembly of the antenna elements.
3. With a separate ground configuration, the reduction of higher-order modes is achieved, which are typically developed in antennas with a large ground plane, thereby reducing the bandwidth and radiation efficiency.
4. Isolation is improved using a decoupling structure. We analyze the effects of short and long stubs on decoupling levels and their role in mitigating coupled currents between the antennas.
5. Additionally, the overall size of the antenna is designed to be compact, making it suitable for portable devices and similar applications.

2. Antenna Geometry

2.1. Antenna Element. The antenna element structure is shown in Figure 1(a), featuring four symmetrical slots, a strip on top of a circular ring-shaped patch, and a truncated ground plane on the back of the substrate to achieve a satisfactory operational frequency band, as illustrated in Figure 1(c). The proposed antenna element has an overall size of $12 \times 10\,\text{mm}^2$ and a substrate thickness of 0.254 mm, made from Rogers RT-5880. This substrate is chosen for its low loss characteristics, evidenced by its low loss tangent of 0.0009 [25], making it suitable for millimeter-wave and higher frequency applications. The back of the proposed antenna element is shown in Figure 1(b). Key dimensions of the proposed antenna structure are listed in Table 1. The

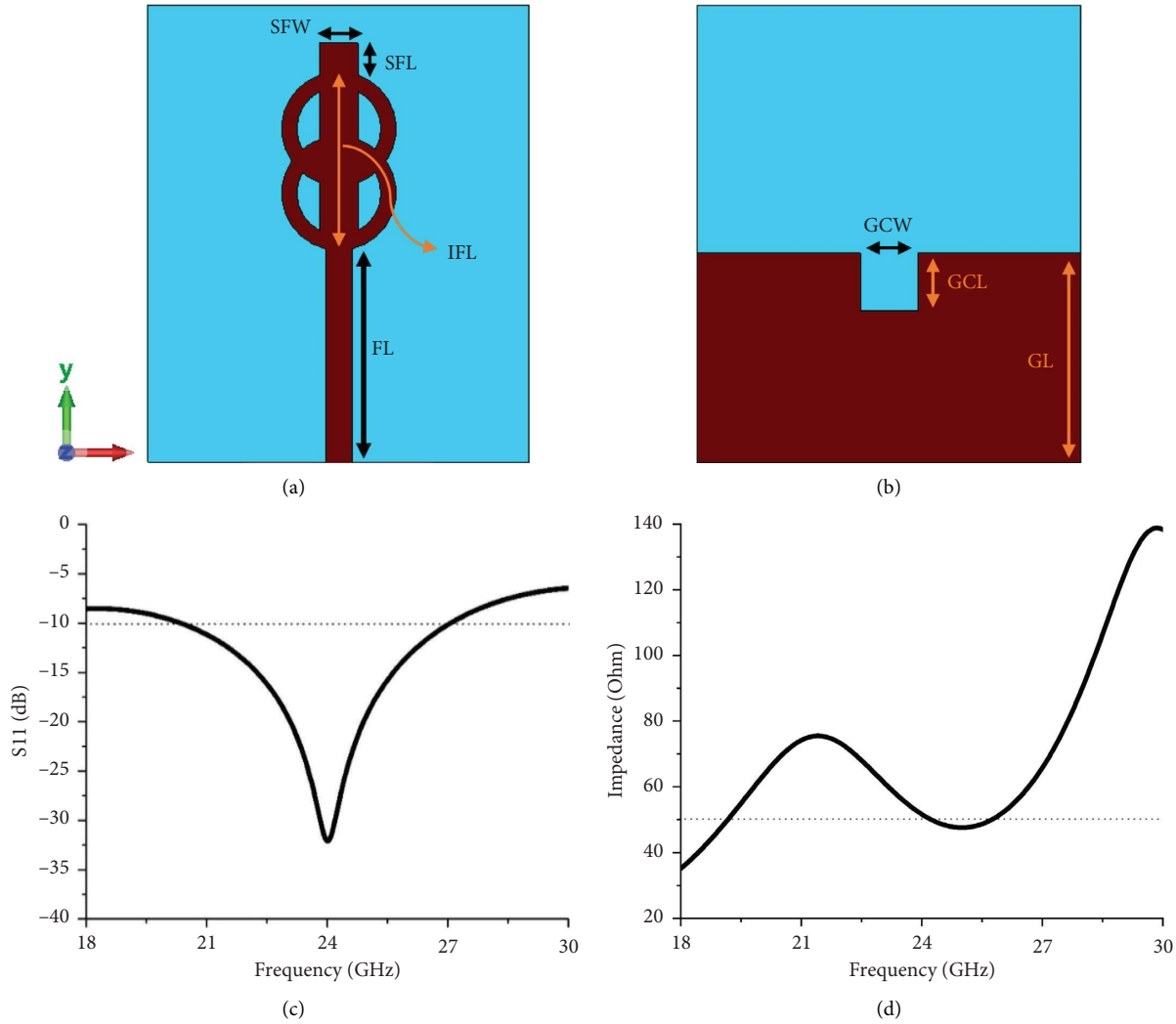

Figure 1: Antenna element structure: (a) front, (b) back, (c) reflection coefficient, and (d) Z-parameter.

Table 1: Key dimensions of the proposed antenna element.

Parameter	Value (mm)
SFW	1.0
SFL	0.8
IFL	4.58
FL	5.6
GCW	1.5
GCL	1.5
GL	5.5

antenna design utilizes a combination of circular patches, with the radius estimated using the equations outlined in [26].

$$R = \frac{F}{\sqrt{1 + (2h/\pi\varepsilon F[\ln(F\pi/2h) + 1.7726])}},$$
$$F = \frac{8.791 \times 10^9}{f\sqrt{\varepsilon}}, \quad (1)$$

where 'R' represents the radius of the patch and "h" is the height of the substrate. While "f" is the resonance frequency, and "ε" denotes the effective dielectric constant of the substrate.

The reflection coefficient of the antenna is crucial, as it directs whether the maximum power is effectively delivered to the antenna. A higher magnitude of this scattering parameter signifies that minimal power is reflected back towards the input, allowing most of the power to be delivered to the antenna and subsequently radiated as electromagnetic fields. As illustrated in Figure 1(c), the reflection coefficient magnitude is less than −30 dB, indicating minimal power reflection losses. The proposed antenna element operates within a bandwidth of 20.317–27.122 GHz, spanning approximately 6.8 GHz. This represents a substantial bandwidth, which is further enhanced when the antenna elements are integrated into the antenna system. Details of these improvements are discussed in the subsequent section. Additionally, the impedance of the antenna element design is illustrated in Figure 1(d). At the fundamental frequency of 24 GHz, the impedance is approximately 50 Ω.

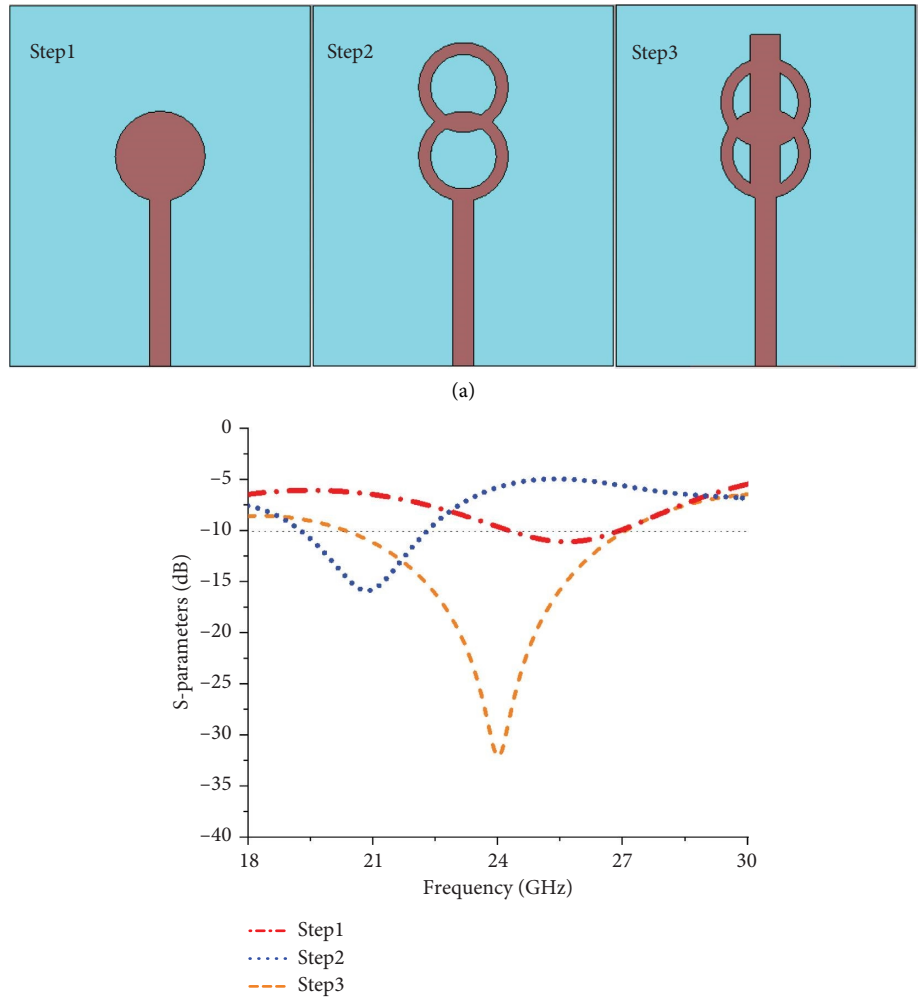

Figure 2: (a) Proposed antenna element design evolution and (b) reflection coefficient comparison.

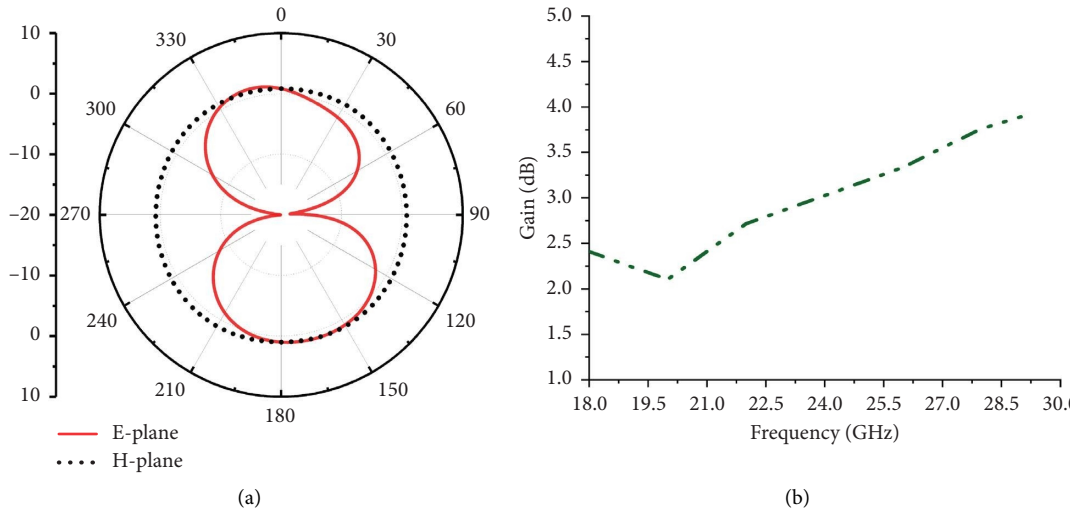

Figure 3: (a) Radiation pattern and (b) gain over frequency.

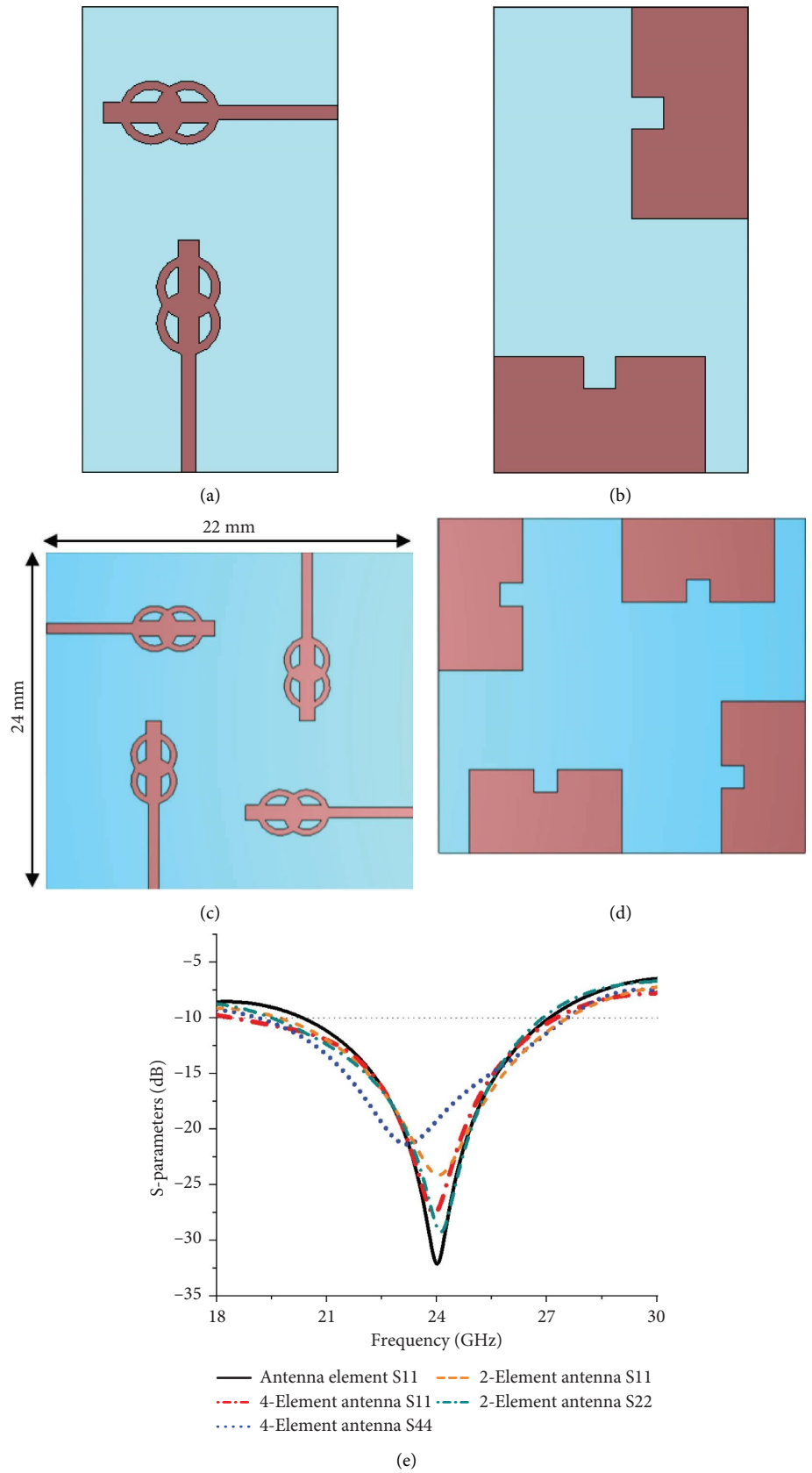

FIGURE 4: Proposed multiport antenna configuration: (a) 2-element front side, (b) 2-element back side, (c) 4-element front side, (d) 4-element back side, and (e) S-parameters comparison.

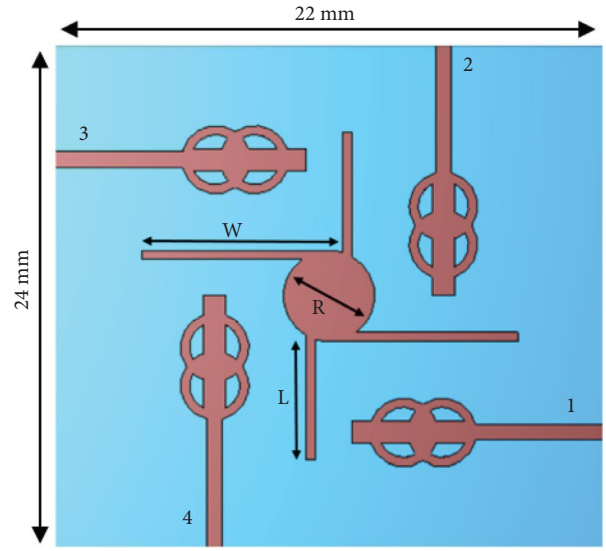

Figure 5: Multiport antenna configuration with a decoupling structure.

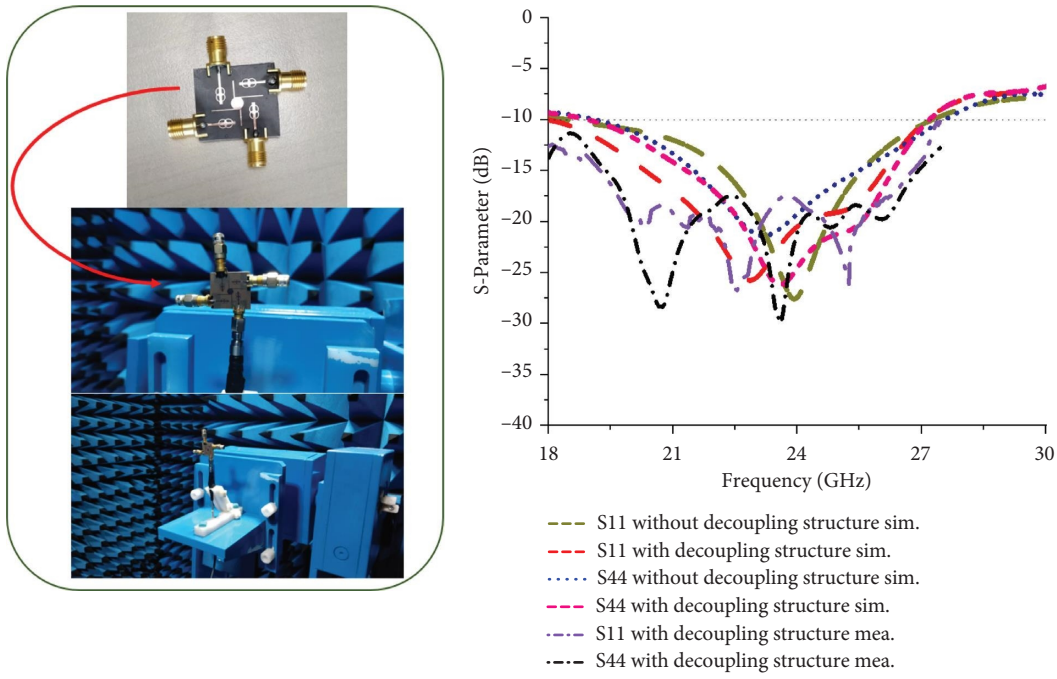

Figure 6: Continued.

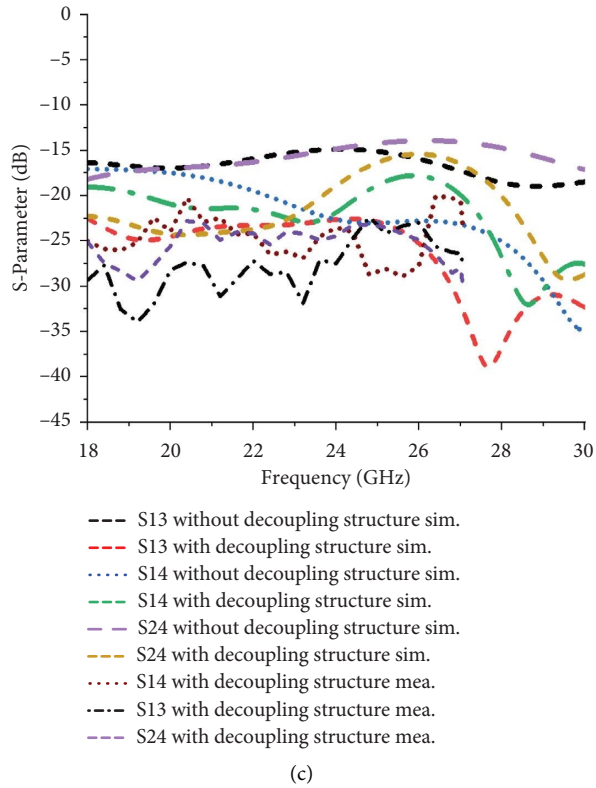

(c)

Figure 6: Proposed multiport antenna configuration: (a) fabricated prototype and experimental setup, (b) reflection coefficient, and (c) transmission coefficient.

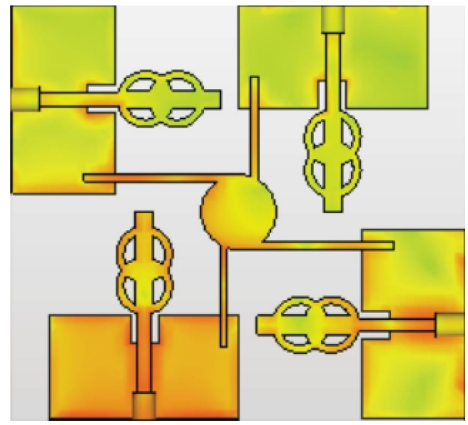

Figure 7: Observation of decoupling through the surface current distribution.

In Figure 2(a), the design evolution of the proposed antenna element is presented. Initially in step 1, a circular-shaped patch is designed which resonates without a better impedance matching and low bandwidth as shown in Figure 2(b). Thus, in step 2, the slots are introduced combined with another circular patch which improves the impedance matching and bandwidth. While in step 3, adding a strip at the center within the circular rings further improves the impedance matching and bandwidth. The gain pattern of the proposed antenna element, shown in Figure 3(a), is presented for both the E and H planes. The radiation pattern, illustrated in Figure 3(b), is observed to be nearly omnidirectional with a gain of approximately 3 dBi at 24 GHz.

2.2. Configuration of a Multiport Antenna. The proposed antenna element is expanded into a multiport configuration (2-elements and then 4-elements), as shown in Figures 4(a), 4(b), 4(c), 4(d). Proper positioning of the antenna elements is crucial for maintaining good isolation between them and preventing performance degradation. To achieve this, a DGS is often employed to create a band-stop effect, mitigating

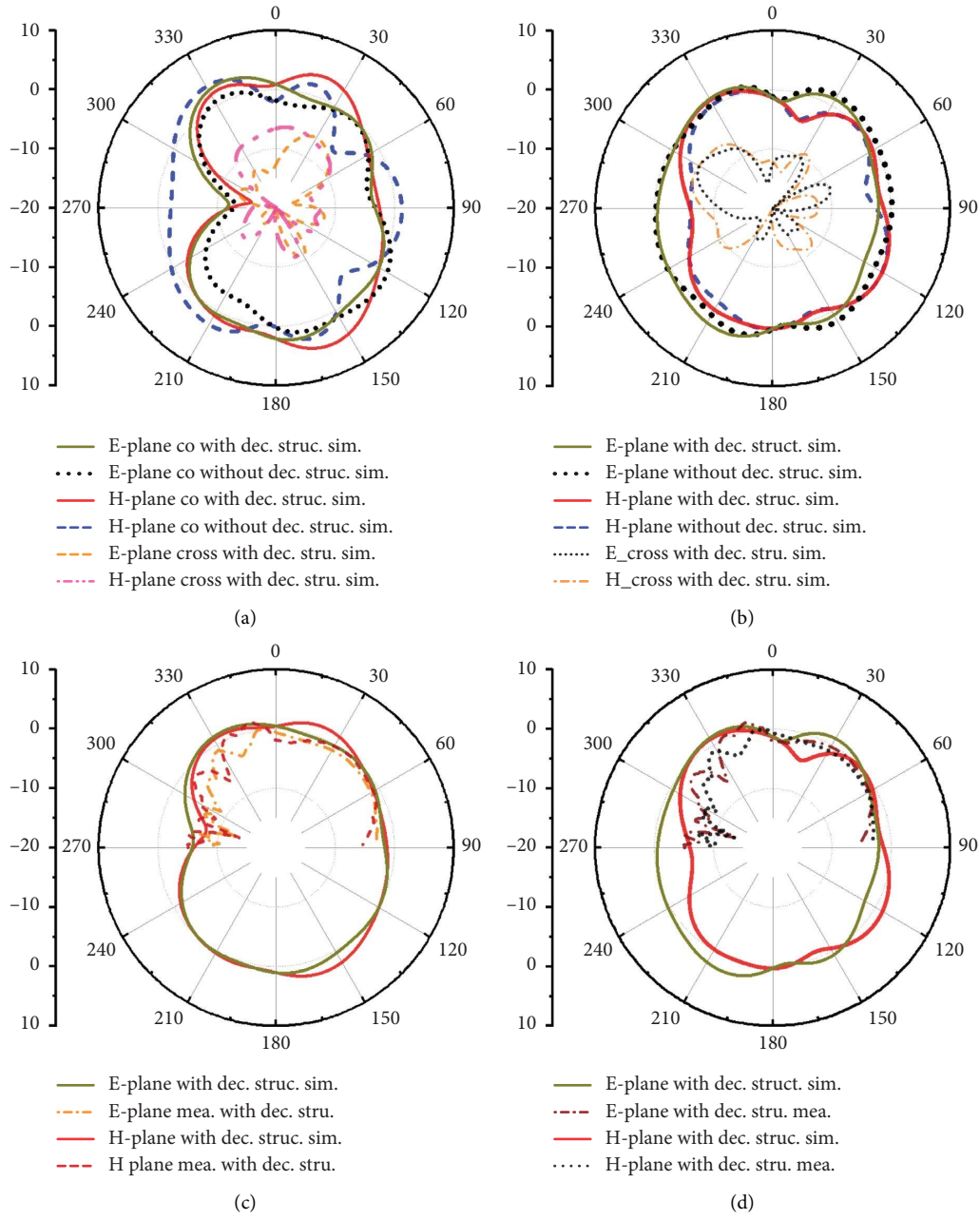

Figure 8: Proposed multiport antenna radiation pattern: (a) element-1 with and with decoupling structure comparison (co and cross-polarized), (b) element-4 with and without decoupling structure comparison (co and cross-polarized), (c) element-1 sim., and mea., results comparison with decoupling structure (co-polarized), and (d) element-4 sim., and mea., results comparison with decoupling structure (co-polarized).

ground currents between antenna elements [27]. Additionally, surface waves diffracted at the edges of a finite ground plane can lead to significant energy loss due to reflections [28]. To address this, using disconnected ground planes can be beneficial. A decoupling network can also improve isolation [29], which is discussed in further detail in the subsequent section. The total size of the proposed multiport antenna configuration is $24 \times 22\,\text{mm}^2$, with a separation of approximately 4.5 mm between the antenna elements. Two defected ground planes are positioned 2 mm from the substrate edge to reduce ground currents between elements. This arrangement of antenna elements and truncated ground planes not only improves isolation but also enhances the bandwidth as shown in Figure 4(e). The antenna element offers a bandwidth of approximately 6.8 GHz, which increases to around 9 GHz in the multiport configuration, benefiting from optimal positioning, assembly, and truncation of the ground planes. More details are discussed in the results section.

2.3. Multiport Antenna Configuration With a Decoupling Structure. Figure 5 shows the proposed multiport antenna configuration with the incorporated decoupling structure.

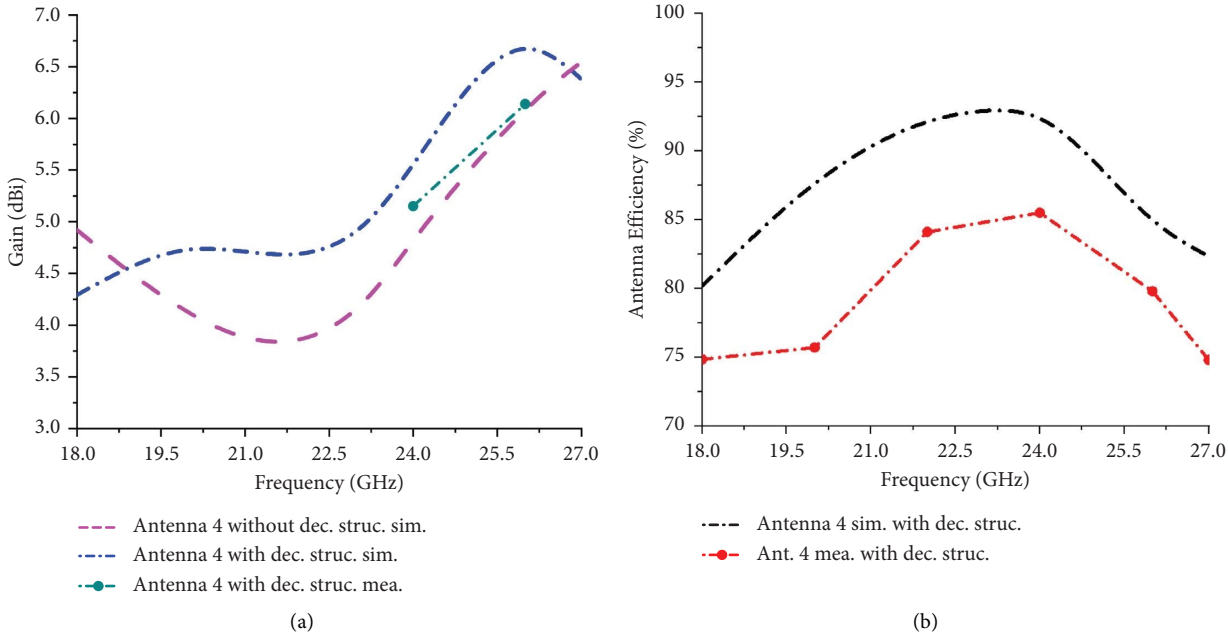

Figure 9: Proposed multiport antenna: (a) gain and (b) efficiency.

Table 2: Gain measurement noted at selected frequency points.

Freq. (GHz)	Gain (dBi)
24	5.15
26	6.14

This structure is designed to minimize the flow of coupled field currents between the antenna elements, thereby enhancing overall antenna performance. The key design parameters for the decoupling structure are: $W = 8.8$ mm, $L = 5.4$ mm, and $R = 2$ mm. The stub lengths are optimized to achieve optimal performance. Due to different defected ground positions for the respective antenna elements, as illustrated in Figure 4(b), the lengths of the diagonal stubs are varied to minimize coupling currents. Additionally, the stubs for antenna elements 2 and 4 are kept shorter than those for antenna elements 1 and 3 to compare their effects on reducing coupling between the elements. Furthermore, a minor improvement in bandwidth is observed after incorporating the decoupling structure, which is discussed in more detail in the results section.

2.4. Comparison of Results for Multiport Antenna With and Without Decoupling Structure. This section compares the performance of the proposed multiport antenna with and without the decoupling structure. Figure 6(a) shows the fabricated prototype of the multiport antenna. Figure 6(b) illustrates the reflection coefficient of the antenna. Operating near 24 GHz, the antenna exhibits a wide bandwidth. The slight variation in the reflection coefficient magnitude between antennas 1 and 4 is due to the different positions of the truncated ground planes. The reflection coefficient magnitude ranges from −25 to −30 dB, indicating minimal power reflection losses. The antenna element offers a bandwidth of approximately 6.8 GHz, which increases to around 9 GHz in the multiport configuration, benefiting from optimal positioning, assembly, and truncation of the ground planes.

The decoupling performance between the antenna elements is illustrated in Figure 6(c). Without the decoupling structure, the scattering parameter S13 shows a decoupling level of approximately −15 dB at 24 GHz. Introducing the decoupling structure improves this to around −25 dB. Notably, stubs between antenna elements 1 and 3 differ in length from those between elements 2 and 4, affecting the decoupling levels. For the decoupling between elements 1 and 4, an improvement is observed from 18 to 24 GHz, but a drop occurs from 24 to 28 GHz due to the differing stub lengths. For elements 2 and 4, the decoupling level without the structure ranges from −15 to −20 dB, improving somewhat with the decoupling structure. The shorter stubs for elements 2 and 4 compared to elements 1 and 3 contribute to these results. The stubs for elements 1 and 3 generally perform better throughout the frequency range. The incorporation of the decoupling structure also leads to a minor bandwidth improvement and enhances the reflection coefficient magnitude at several frequencies.

Figure 7 reveals the surface current distribution for antenna element 4. At 23 GHz, current distribution is concentrated around this element, with low coupling currents around elements 2 and 3 due to the decoupling structure (particularly the long stubs). Some increased coupling current is observed around element 1, attributed to the shorter stub between elements 1 and 4. The long stubs effectively mitigate coupled currents.

Radiation patterns for the proposed multiport antenna in the E and H planes at 23 GHz are illustrated in Figure 8, while Figure 9(a) shows the gain plot. The maximum gain,

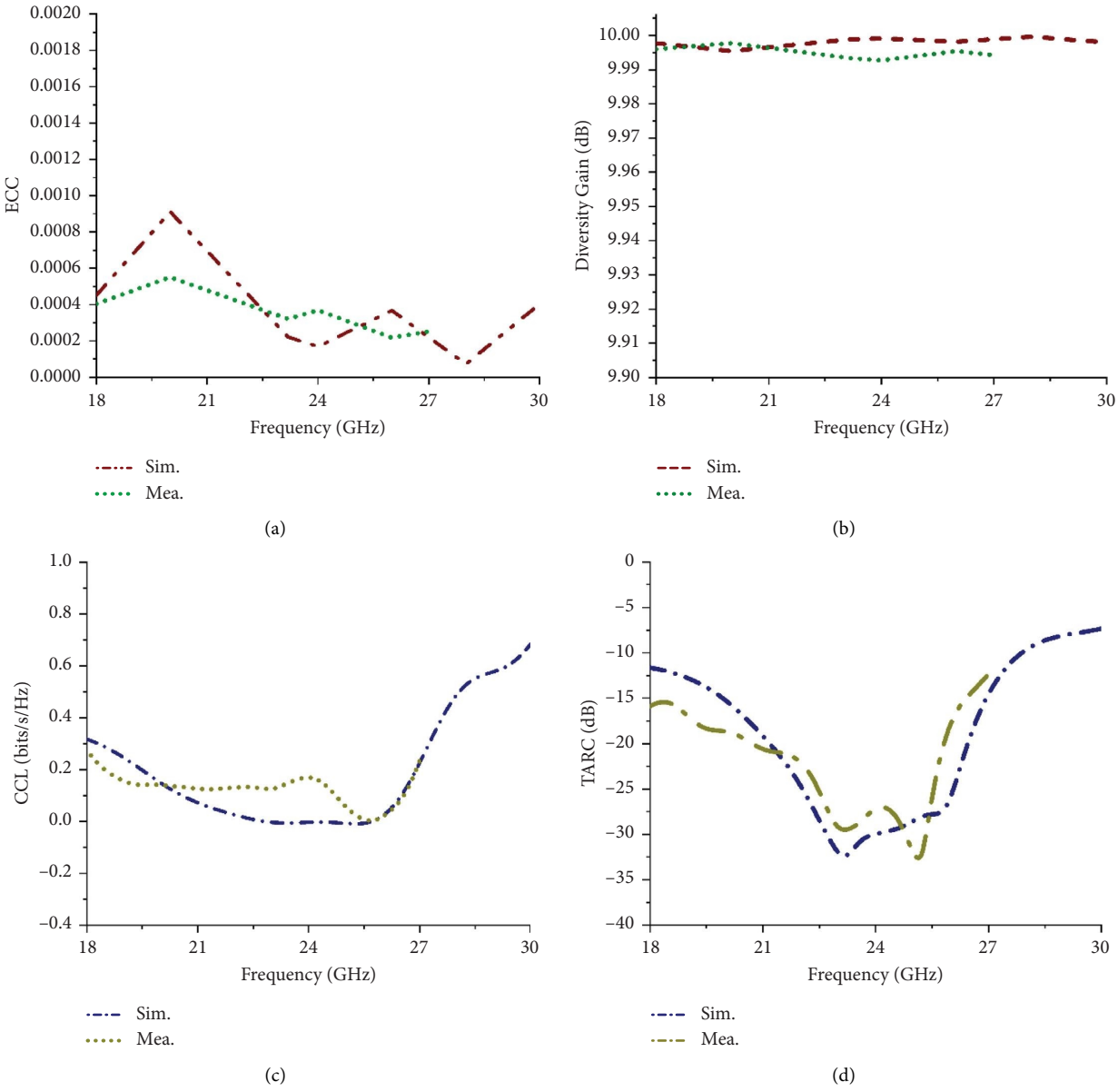

Figure 10: Proposed multiport antenna performance metrics: (a) ECC, (b) DG, (c) CCL, and (d) TARC.

with and without the decoupling structure, ranges from 6 to 6.8 dBi, with the decoupling structure improving gain by suppressing unwanted coupling fields. The radiation efficiency of antenna 4 is shown in Figure 9(b), exceeding 75% within the operating bandwidth. Measured results, indicated by "mea" in the figures, are in good agreement with the simulations, with minor discrepancies due to fabrication errors, soldering, and environmental noise.

In Table 2, the gain measurement noted at selected frequency points is provided. Figure 10 displays performance metrics including the total active reflection coefficient (TARC), diversity gain (DG), envelope correlation coefficient (ECC), and channel capacity loss (CCL) for the multiport antenna with the decoupling structure. The ECC, calculated using the far-field method described in [30], is less than 0.0009, indicating minimal coupling between the antenna elements. The DG of the antenna is approximately 10 dB, suggesting strong directional performance. Meanwhile, the CCL is below 0.4 bits/s/Hz, reflecting efficient use of the available bandwidth. Additionally, the TARC is below −10 dB, which signifies good impedance matching and reduced signal reflection. Overall, these results collectively demonstrate the satisfactory performance of the proposed multiport antenna in terms of minimal element coupling, high directivity, efficient bandwidth utilization, and effective impedance matching.

2.5. Multiport Antenna With a Connected Ground Plane. This section presents the performance of the proposed antenna with a connected ground plane. The structure which is used as a decoupling structure is also utilized to

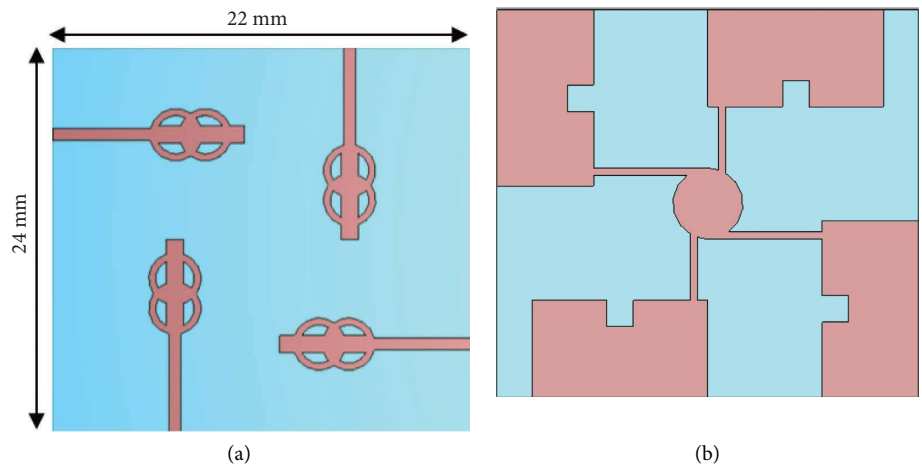

Figure 11: Proposed multiport antenna configuration with connected ground plane: (a) front side and (b) back side.

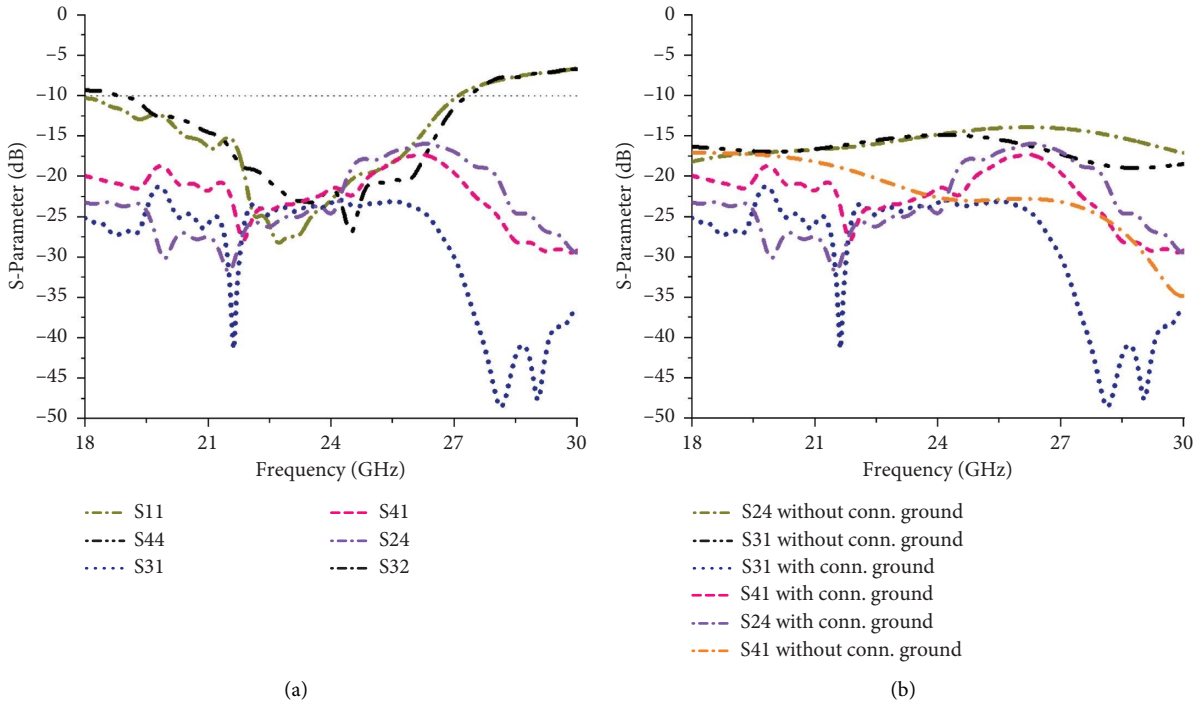

Figure 12: (a) S-parameters of multiport antenna with a connected ground plane and (b) with and without connected ground plane, isolation comparison.

connect the ground planes with each other. In Figure 11, the geometry of the proposed multiport antenna is shown with a connected ground plane. While the S-parameters are presented in Figure 12(a). Overall, the isolation is better at some frequency points ranging from 18 to 25 GHz, when the ground plane is connected than the antenna without connected ground plane as shown in Figure 12(b). However, at some frequency points, the response is nearly same with and without connected ground plane. Overall, the results are satisfactory with a connected ground plane and can be potentially utilized for the K-band and 5 G applications.

3. Performance Comparison of the Proposed Multiport Antenna With Other Multiport Antennas

Table 3 presents a performance comparison of mm-wave and high-frequency band antennas from the literature. The comparison is based on the electrical size of the antennas at their lowest operating frequency within the desired bandwidth. For instance, the antenna design in reference [20] covers a bandwidth from 25.5 to 29.6 GHz with an overall size of 30×35 mm^2. It achieves isolation above 17 dB and an envelope correlation coefficient (ECC) of less than 0.01.

Table 3: Proposed multiport antenna performance comparison with other multiport antennas.

Ref.	Antenna size	Bandwidth	Isolation (dB)	ECC	Decoupling method	Application
[17]	35×40 (mm^2) $3.27\lambda_0 \times 3.74\lambda_0$	24.1–30.9 (GHz)	> 30	< 0.18	Decoupling structure	5 G
[19]	20.5×12 (mm^2) $1.75\lambda_0 \times 1.02\lambda_0$	25.5–30 (GHz)	32–43	—	Antennas orientation	mm-wave
[20]	30×35 (mm^2) $2.55\lambda_0 \times 2.98\lambda_0$	25.5–29.6 (GHz)	> 17 dB	< 0.01	DGS	5 G
[21]	30×30 (mm^2) $2.7\lambda_0 \times 2.7\lambda_0$	27–29.4 (GHz)	> 29	< 0.16	DGS	5 G
[22]	52×23 (mm^2) $4.42\lambda_0 \times 1.95\lambda_0$	24–30 (GHz)	> 24	< 0.0013	Metamaterial	Millimeter-wave 5 G
[24]	53×31.7 (mm^2) $3.97\lambda_0 \times 2.38\lambda_0$	22.5–50 (GHz)	> 20	0.12	EBG reflector	5 G
[31]	49×45 (mm^2)	5.18–19.016 (GHz)	20	0.0001	Antennas orientation	5 G, UWB, WLAN/Wi-Fi
[32]	250×259 (um^2)	2.3–2.7, 5.5–8.9 (THz)	30	0.001 and 0.00001	FSS wall	THz
[33]	120×120 (um^2)	0.65–10.7 (THz)	17	0.01457	Antennas orientation	IoT, 6 G
[34]	40.4×20 (mm^2)	27.6–30.3 and 33.4–40.4 (GHz)	20	0.0001	Slots and tilting radiators	5 G
[35]	24×20 (mm^2)	24.10–27.18 and 33–44.13 (GHz)	> 16	< 0.1	Antennas orientation	5 G
Prop.	24×22 $1.44\lambda_0 \times 1.32\lambda_0$	18–27 (GHz)	> 20	< 0.0009	Decoupling structure	K-band, 5 G

However, its operational bandwidth is only about 4 GHz. Similarly, the antenna design in reference [21] has a size of $30 \times 30\ mm^2$ and operates over a bandwidth of 27–29.4 GHz, with isolation above 29 dB and an ECC of less than 0.16. While it has good isolation, the ECC is relatively high and the operational bandwidth is limited to around 2.4 GHz. Reference [22] describes an antenna design with a size of $52 \times 23\ mm^2$, covering a bandwidth of approximately 6 GHz from 24 to 30 GHz. It offers isolation above 24 dB and an ECC of less than 0.0013. Despite the satisfactory bandwidth and low ECC, the size of the antenna is somewhat larger. Reference [24] details an antenna design with an overall size of $53 \times 31.7\ mm^2$ and a wide operational bandwidth ranging from 22.5 to 50 GHz. It provides isolation greater than 20 dB with an ECC of 0.12. Although it covers a broad frequency range, its size is large, and the ECC is relatively high. The inclusion of an EBG reflector also adds complexity to the design. In reference [31–33], the multiport antennas operating at mm-wave and THz frequency bands are reported. Where some FSS or varying antennas orientation method is utilized to improve the isolation. But rather the complexity of the design is increased or low isolation is attained. In reference [34, 35], multiport antennas are proposed for 5G applications. The slots are introduced in the ground plane, tilting the radiators, or varying antenna elements orientation is helpful to achieve a reasonable isolation. But with either increasing geometrical complexity by involving power dividers or glass materials.

Overall, most of the antenna designs in the literature face issues related to limited bandwidth, design complexity, or compactness, along with lower isolation levels. In contrast, the proposed multiport antenna in this study covers the entire K-band (18–27 GHz) and the 5 G band (24.5–27.5 GHz). The design achieves a significant improvement in bandwidth, extending up to approximately 9 GHz, by optimizing the positioning, assembling, and truncating of the ground planes. This results in better reflection coefficient magnitude, indicating minimal reflection losses and efficient power delivery. Additionally, the proposed antenna incorporates a decoupling structure with four stubs of varying lengths, which enhances isolation and performance across the operating band. The study also explores the impact of different stub lengths on decoupling, contributing to a deeper understanding of decoupling structures in multiport antennas on a common substrate. In summary, the proposed multiport antenna demonstrates wide bandwidth, optimal gain, improved isolation, and high efficiency. It is well-suited for K-band and 5G applications, offering significant advantages over existing designs.

4. Conclusion

In this paper, a compact multiport antenna configuration is achieved by assembling four antenna elements. The design incorporates truncated ground planes and symmetrical slots in the radiating structures to attain a wide bandwidth. Additionally, the inclusion of a decoupling structure further enhances the bandwidth and improves the reflection coefficient magnitude, indicating minimal reflection losses. To ensure high isolation within the desired frequency band, a decoupling structure with four stubs of varying lengths is used between the radiating elements, and the effect of different stub lengths on decoupling performance is analyzed. The proposed antenna exhibits a low ECC of less than 0.0009, a wide operational bandwidth spanning from 18 to 27 GHz, optimum gain, high isolation (> 20 dB), low CCL (< 0.4 bits/s/Hz), and better efficiency. These attributes highlight the potential of the proposed multiport antenna for K-band and 5 G applications.

Data Availability Statement

All data generated or analyzed during this study is included in this article.

Disclosure

All of the figures, materials, and data within the manuscript are original and owned by authors.

Conflicts of Interest

The authors declare no conflicts of interest.

Author Contributions

D.A.S., S.H.K. contributed in conceptualization; D.A.S., S.H.K., T.A. proposed methodology; D.A.S., S.H.K., T.A. used software; D.A.S., S.H.K., T.A., M.I.A. contributed in validation; T.A., M.I.A., M.R.K. contributed in investigation; M.I.A., M.R.K, A.D.A., H.E. provided resources; D.A.S., S.H.K. wrote original draft; D.A.S., S.H.K., T.A., M.I.A., M.R.K., A.D.A., H.E. contributed in review and editing the manuscript; M.R.K., A.D.A., H.E. supervised. All authors have read and agreed to the published version of the manuscript.

Funding

The authors sincerely appreciate the funding for this research work from Princess Nourah bint Abdulrahman University Researchers Supporting Project number (PNURSP2025R51), Princess Nourah bint Abdulrahman University, Riyadh, Saudi Arabia.

References

[1] M. Malekzadeh, "Performance Prediction and Enhancement of 5G Networks Based on Linear Regression Machine Learning," *EURASIP Journal on Wireless Communications and Networking* 2023, no. 1 (2023): 74, https://doi.org/10.1186/s13638-023-02282-z.

[2] G. Mingming, W. Jun, and N. Jingchang, "Quad MIMO Millimeter Wave Antenna for 5G Applications," in *IEEE 13th International Symposium on Antennas, Propagation and EM Theory (ISAPE)* (Zhuhai, China, 2021), 1–3, https://doi.org/10.1109/isape54070.2021.9752885.

[3] M. I. Rochman, V. Sathya, D. Fernandez, et al., "A Comprehensive Analysis of the Coverage and Performance of 4G

and 5G Deployments," *Computer Networks* 237 (2023): 110060, https://doi.org/10.1016/j.comnet.2023.110060.

[4] Y. Wang and F. Xu, "Shared Aperture 4G LTE and 5G mm-Wave Antenna in Mobile Phones With Enhanced mm-Wave Radiation in the Display Direction," *IEEE Transactions on Antennas and Propagation* 71, no. 6 (2023): 4772–4782, https://doi.org/10.1109/tap.2023.3262971.

[5] N. Kishore and A. Senapati, "5G Smart Antenna for IoT Application: A Review," *International Journal of Communication Systems* 35, no. 13 (2022): 5241, https://doi.org/10.1002/dac.5241.

[6] S. Tariq, S. I. Naqvi, N. Hussain, and Y. Amin, "A Metasurface-Based MIMO Antenna for 5G Millimeter-Wave Applications," *IEEE Access* 9 (2021): 51805–51817, https://doi.org/10.1109/access.2021.3069185.

[7] R. S. Aziz, S. Koziel, L. Leifsson, and S. Szczepanski, "Novel Versatile Topologies and Design Optimization of Wide-Bandstop Frequency Selective Surfaces for X-Band, Ku-Band and Millimeter-Wave Applications," *Scientific Reports* 13, no. 1 (2023): 1952, https://doi.org/10.1038/s41598-023-28922-4.

[8] M. L. Hakim, T. Alam, A. F. Almutairi, M. F. Mansor, and M. T. Islam, "Polarization Insensitivity Characterization of Dual-Band Perfect Metamaterial Absorber for K Band Sensing Applications," *Scientific Reports* 11, no. 1 (2021): 17829, https://doi.org/10.1038/s41598-021-97395-0.

[9] S. Kumar, N. n. Tiwari, M. Arif A, A. K. Dwivedi, and V. Singh, "MIMO Antenna With Low Mutual Coupling and High Gain for N257-Band 5G Mm-Wave," in *IEEE 13th International Symposium on Advanced Topics in Electrical Engineering (ATEE)* (Bucharest, Romania, 2023), 1–5, https://doi.org/10.1109/atee58038.2023.10108208.

[10] H. V. Singh, D. V. S. Prasad, and S. Tripathi, "Self-Isolated MIMO Antenna Using Mixed Coupling by Close Coupling Technique," *Scientific Reports* 13, no. 1 (2023): 5636, https://doi.org/10.1038/s41598-023-32364-3.

[11] C. Liu, T. Zhu, J. Qian, L. Zhang, and X. Zhang, "Convex Optimization Algorithm for Maximizing Directivity of Conformal Array With DRR Constraint," *International Journal of Antennas and Propagation* 2024, no. 1 (2024): 9320514, https://doi.org/10.1155/2024/9320514.

[12] P. K. Panda and D. Ghosh, "Isolation and Gain Enhancement of Patch Antennas Using EMNZ Superstrate," *AEU-International Journal of Electronics and Communications* 86 (2018): 164–170, https://doi.org/10.1016/j.aeue.2018.01.037.

[13] M. Alibakhshikenari, B. S. Virdee, C. H. See, et al., "Study on Isolation Improvement Between Closely-Packed Patch Antenna Arrays Based on Fractal Metamaterial Electromagnetic Bandgap Structures," *IET Microwaves, Antennas & Propagation* 12, no. 14 (2018): 2241–2247, https://doi.org/10.1049/iet-map.2018.5103.

[14] K. Du, Y. Wang, and Y. Hu, "Design and Analysis on Decoupling Techniques for MIMO Wireless Systems in 5G Applications," *Applied Sciences* 12, no. 8 (2022): 3816, https://doi.org/10.3390/app12083816.

[15] M. Hussain, W. A. Awan, E. M. Ali, et al., "Isolation Improvement of Parasitic Element-Loaded Dual-Band MIMO Antenna for Mm-Wave Applications," *Micromachines* 13, no. 11 (2022): 1918, https://doi.org/10.3390/mi13111918.

[16] P. Kumar, S. Pathan, S. Vincent, et al., "A Compact Quad-Port UWB MIMO Antenna With Improved Isolation Using a Novel Mesh-Like Decoupling Structure and Unique DGS," *IEEE Transactions on Circuits and Systems II: Express Briefs* 70, no. 3 (2023): 949–953, https://doi.org/10.1109/tcsii.2022.3220542.

[17] P. Shariff B G, A. A. Naik, T. Ali, et al., "High-Isolation Wide-Band Four-Element MIMO Antenna Covering Ka-Band for 5G Wireless Applications," *IEEE Access* 11 (2023): 123030–123046, https://doi.org/10.1109/access.2023.3328777.

[18] A. Ahmad, Dy. Choi, and S. Ullah, "A Compact Two Elements MIMO Antenna for 5G Communication," *Scientific Reports* 12, no. 1 (2022): 3608, https://doi.org/10.1038/s41598-022-07579-5.

[19] F. Taher, H. A. Hamadi, M. S. Alzaidi, et al., "Design and Analysis of Circular Polarized Two-Port MIMO Antennas With Various Antenna Element Orientations," *Micromachines* 14, no. 2 (2023): 380, https://doi.org/10.3390/mi14020380.

[20] M. Khalid, S. Iffat Naqvi, N. Hussain, et al., "4-Port MIMO Antenna With Defected Ground Structure for 5G Millimeter Wave Applications," *Electronics* 9, no. 1 (2020): 71, https://doi.org/10.3390/electronics9010071.

[21] M. M. Kamal, S. Yang, X.-C. Ren, et al., "Infinity Shell Shaped MIMO Antenna Array for mm-Wave 5G Applications," *Electronics* 10, no. 2 (2021): 165, https://doi.org/10.3390/electronics10020165.

[22] S. S. Al-Bawri, M. T. Islam, T. Shabbir, G. Muhammad, M. S. Islam, and H. Y. Wong, "Hexagonal Shaped Near Zero Index (NZI) Metamaterial Based MIMO Antenna for Millimeter-Wave Application," *IEEE Access* 8 (2020): 181003–181013, https://doi.org/10.1109/access.2020.3028377.

[23] W. Ali, S. Das, H. Medkour, and S. Lakrit, "Planar Dual-Band 27/39 GHz Millimeter-Wave MIMO Antenna for 5G Applications," *Microsystem Technologies* 27, no. 1 (2020): 283–292, https://doi.org/10.1007/s00542-020-04951-1.

[24] A. A. R. Saad and H. A. Mohamed, "Printed Millimeter-Wave MIMO-Based Slot Antenna Arrays for 5G Networks," *AEU-International Journal of Electronics and Communications* 99 (2019): 59–69, https://doi.org/10.1016/j.aeue.2018.11.029.

[25] R. K. Raj, V. K. Sharma, P. Joshi, H. R. Choudhary, A. Tripathi, and Jayesh, "Comparative Analysis of Dielectric Substrate Materials (FR-4 & RT/Duriod 5880) for Antenna Array (8∗1) Designing," *Materials Today: Proceedings* 74 (2023): 172–178, https://doi.org/10.1016/j.matpr.2022.08.041.

[26] M. I. Khattak, A. Sohail, U. Khan, Z. Barki, and G. Witjaksono, "Elliptical Slot Cicular Patch Antenna Array With Dual Band Behaviour for Future 5G Mobile Communication Networks," *Progress in Electromagnetics Research C* 89 (2019): 133–147, https://doi.org/10.2528/pierc18101401.

[27] M. M. Hasan, M. T. Islam, T. Alam, A. Alzamil, and M. S. Soliman, "Electromagnetic Coupling Shielding in Compact MIMO Antenna Using Symmetric T-Shaped Metamaterial Structure for 5G Communications," *Optics & Laser Technology* 169 (2024): 110046, https://doi.org/10.1016/j.optlastec.2023.110046.

[28] M. Alibakhshikenari, B. S. Virdee, and E. Limiti, "Study on Isolation and Radiation Behaviours of a 34 × 34 Array-Antennas Based on SIW and Metasurface Properties for Applications in Terahertz Band Over 125–300 GHz," *Optik* 206 (2020): 163222, https://doi.org/10.1016/j.ijleo.2019.163222.

[29] A. Alfakhri, "Dual Polarization and Mutual Coupling Improvement of UWB MIMO Antenna With Cross Shape Decoupling Structure," *E-Prime-Advances in Electrical Engineering, Electronics and Energy* 4 (2023): 100130, https://doi.org/10.1016/j.prime.2023.100130.

[30] O. Khan, S. Khan, S. N. K. Marwat, N. Gohar, M. Bilal, and M. Dalarsson, "A Novel Densely Packed 4 × 4 MIMO Antenna Design for UWB Wireless Applications," *Sensors* 23, no. 21 (2023): 8888, https://doi.org/10.3390/s23218888.

[31] P. A. Gajbhiye, S. P. Singh, and M. K. Sharma, "Computationally Optimized Multi-Port Antenna Systems for WLAN/Wi-Fi (IEEE 802.11a/h/j/n/Ac/Ax), 5G (Mid-Band), and UWB Applications," *International Journal of Communication Systems* (2024): https://doi.org/10.1002/dac.5985.

[32] M. K. Sharma, A. Sharma, and R. Kumari, "A CPW THz-MIMO Antenna with Reduced Mutual Coupling Using Frequency Selective Surface for Future Wireless Applications," *Optical Materials* 148 (2024): 114929, https://doi.org/10.1016/j.optmat.2024.114929.

[33] A. Sharma, D. Gangwar, and M. K. Sharma, "Easily Extendable Optically Transparent Multi-Port Dual Polarized Wideband THz-MIMO Antenna for Biomedical Sensing, Industry 4.0, IoT, and 6G Applications," *Optical and Quantum Electronics* 55, no. 14 (2023): 1282, https://doi.org/10.1007/s11082-023-05566-2.

[34] Y.-F. Tsao, A. Desai, and H.-T. Hsu, "Dual-Band and Dual-Polarization CPW Fed MIMO Antenna for Fifth-Generation Mobile Communications Technology at 28 and 38 GHz," *IEEE Access* 10 (2022): 46853–46863, https://doi.org/10.1109/access.2022.3171248.

[35] A. Desai, C. D. Bui, J. Patel, T. Upadhyaya, G. Byun, and T. K. Nguyen, "Compact Wideband Four Element Optically Transparent MIMO Antenna for mm-Wave 5G Applications," *IEEE Access* 8 (2020): 194206–194217, https://doi.org/10.1109/access.2020.3033314.